Journal of
Nanomedicine & Nanotechnology

López et al., J Nanomed Nanotechnol 2015, 6:1
DOI: 10.4172/2157-7439.1000255

Research Article Open Access

Inclusion of $FeCl_3$ in Sol-Gel TiO_2: Spectroscopic Studies

López T[1,2,3], Moreno A[2], Ortiz-Islas E[1,4], Pecchi G[5], Bersani D[6], Lottici PP[6], Montes M[7], Cuevas JL[1,4]*, Alfaro P[1,4], Morales A[4] and Novaro O[3,8]

[1]*Universidad Autónoma Metropolitana, Xochimilco, Calzada del Hueso No. 1100, Coyoacán, Villa Quietud, C.P. 04960 D.F., México*
[2]*Universidad Autónoma Metropolitana, Iztapalapa, San Rafael Atlixco 186, Vicentina, C.P. 09340, D.F., México*
[3]*Instituto de Física, Departamento de Física Teórica, Universidad Nacional Autónoma de México, Apartado Postal 70-360, C.P. 04510, D.F., México*
[4]*Instituto Nacional de Neurología y Neurocirugía, Departamento de Nanotecnología, México*
Avenida Insurgentes Sur 3877, La Fama, C.P. 14269, D.F., México
[5]*Universidad de Concepción, Facultad de Ciencias Químicas, Edmundo Larenas, 129, Casilla 160-C, Concepción, Chile*
[6]*University of Parma, Physics Department, Parco Area delle Scienze, 7A, 43100 Parma, Italy*
[7]*Universidad del País Vasco, Departamento de Físico Química, Paseo Manuel de Lardizábal, 3-20018 Donostia-San Sebastián, Spain*
[8]*El Colegio Nacional, Donceles 104, Centro Histórico, D.F., México*

Abstract

Utilizing a sol-gel process, Fe-TiO_2 materials containing 0.1, 1, 5 and 10% weight of iron were prepared at pH 3 or pH 9 using HCl or NH_4OH as hydrolysis catalyst respectively. Thenceforth, the samples were annealed at 200°C, 400°C, 600°C and 800°C under airflow during 4 hours and characterized by X-ray diffraction, N_2 adsorption-desorption (BET), infrared spectroscopy (FTIR), X-ray photoelectron spectroscopy (XPS), Raman spectroscopy and Electron Paramagnetic Resonance (EPR). The catalytic activity of the materials was tested on a toluene combustion reaction. The results show that the cogelled iron with n-titanium butoxide slows down the anatase crystal growth. Samples of increasing iron content generate crystal size reduction. This effect is stronger passing from 0.1% to 5% Fe, but becomes weaker from 5% to 10% Fe.

Keywords: Sol-gel; Nanobiocatalyst; Titania

Introduction

Titanium (Ti), is one of the most abundant elements in the earth's crust with a concentration of 4400 mg/kg [1]. It has great affinity with oxygen and other elements forming interesting compounds such as metallic Ti, $TiCl_4$, and Titania (TiO_2). TiO_2 is most widely used in everyday life, as pigments, paints, coatings, plastics, cosmetics, paper, inks, medicine and the pharmaceutical industry [1-4]. TiO_2 is a photo-excited semiconductor that exists as three different polymorphs; anatase, rutile and brookite [4]. Rutile is the most stable form of TiO_2. Typically, the metastable anatase and brookite polymorphs will transform to the thermodynamically stable rutile at temperatures exceeding ~600°C. TiO_2 as a photocatalitic material is widely used for decomposition of toxic organic compounds. The band gap of the more active photocatalytic titania phase, anatase, is 3.1 eV [5], which requires UV irradiation ($\lambda \geq 387$ nm) [6,7]. In order to enhance the catalytic properties, TiO_2 has been doped with different transitions metals such as: Cu, Fe, Ag, and precious metals [8-12] which make that absorption edge shift to the visible region. Iron is a very important requirement for the formation of red blood cells in the human body. It forms a major portion of ftalocianine molecules as hemoglobin. It is also required for hemoglobin synthesis. Iron liberated from senescent red blood cells is normally retained and reutilized. The liver stores ferritin as the primary physiologic source of reserve iron in the body. Iron deficiency first attacks the storage iron in the body, and its depletion is thought to be relatively non-symptomatic, although some vague and non-specific symptoms have been associated with it. High iron levels disturb cells, increase oxidative stress [8], and it can be toxic.

Serum contains a small amount of iron 14-32 μmol/L (males) and 10-28 μmol/L (females) which is bound to the globulin fraction of serum proteins. The physical role of this protein bound iron is the transportation of iron in the body. Low values of serum iron are found in hemorrhagic and hypochromic types of anemia, while high values are found in pernicious anemia. High levels have been associated to parenchymal brain damage, methemoglobinemia and hemosiderosis [8]. It is well known that the photocatalytic activity of TiO_2 depends strongly of the preparation methods and post-treatment conditions, since they have a decisive influence on its chemical and physical properties [9]. In this work, we prepared sol-gel Fe-TiO_2 materials with 0.1, 1.0, 5.0 and 10.0% in weight of iron. We studied the nanomaterials by X-ray diffraction, N_2 adsorption-desorption (BET), Infrared spectroscopy (FTIR), Raman spectroscopy (Figure 1). Afterwards, the combustion toluene reaction was used to confirm that these materials are capable to easily break C-C and C-H bonds, reaching total combustion, liberating CO_2 and H_2O. Costas G. Hadjipanayis et al. made a review about inorganic nanoparticle applications to biology for attacking cancer cells and different tissues, all of these were made with different method [10]. Nevertheless, Saba Ahmad et. al. in the Canadian Chemical Transactions this year, reports that Fe_2O_3-SnO_2 nanoparticles synthetized by the hydrothermal method using several concentrations of sodium dodecyl sulfate (SDS) as surfactant, were proved in some bacteria rupturing the DNA strain [11]. The difference with our nanomaterials is the use of the soft chemistry sol-gel process, having 0.1, 1.0, 5.0 and 10.0% Fe (wt) cogelled in TiO_2. In addition, this method permits to obtain nanomaterials with a high number of punctual defects such as hydroxyl, using low iron concentrations to break C-C, C-N bonds of DNA (Figure 2) as will be discussed in this paper.

Materials and Methods

Chemical duty

- HCl (J.T: Baker 98%)

***Corresponding author:** Cuevas JL, Universidad Autónoma Metropolitana, Xochimilco, Calzada del Hueso No. 1100, Coyoacán, Villa Quietud, C.P. 04960 D.F., México, Tel: 52-55-5483-400; E-mail: jcuevasf@gmail.com

Received November 04, 2014; **Accepted** December 16, 2014; **Published** January 01, 2015

Citation: López T, Moreno A, Ortiz-Islas E, Pecchi G, Bersani D, et al. (2015) Inclusion of $FeCl_3$ in Sol-Gel TiO_2: Spectroscopic Studies. J Nanomed Nanotechnol 6: 255. doi: 10.4172/2157-7439.1000255

Copyright: © 2015 López T, et al. This is an open-access article distributed under the terms of the Creative Commons Attribution License, which permits unrestricted use, distribution, and reproduction in any medium, provided the original author and source are credited.

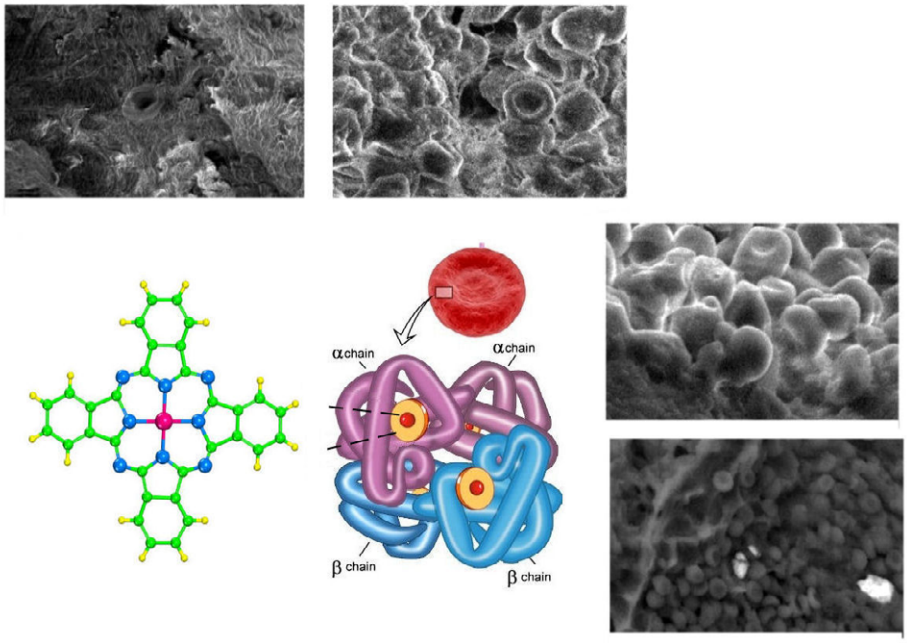

Figure 1: Electronic micrographics of hemoglobin and scheme of hemoglobin molecule (ftalocianine molecule). Where the yellow, green, blue and pink spheres represent atoms of hydrogen, carbon, nitrogen and iron, respectively.

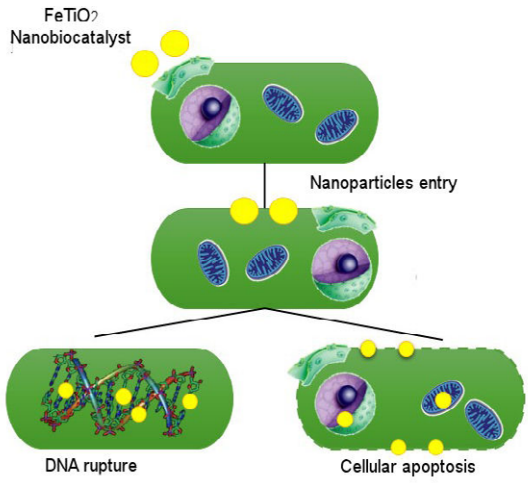

Figure 2: DNA cracking by Fe-TiO_2 nanoparticles.

- NH_4OH (J.T: Baker 98%)
- Titanium tert-butoxide (Strem Chemical 98% in butanol)
- Absolute ethylic alcohol (J.T: Baker 99.9%)
- $FeCl_3.4H_2O$ (J.T: Baker 99%)
- $Fe(NH_4)_2(SO_4)_2$ (J.T: Baker 99%)
- Deionized water

Fe-TiO_2 at 0.1, 1.0, 5.0 and 10.0% in weight were prepared by the sol-gel method depicted to in Figure 3. In a glass reflux system at room temperature, we added deionized water, ethylic alcohol and the necessary ferric salt to obtain the correct amount. The pH was adjusted at 3 or 9 with hydrochloric acid or ammonium hydroxide respectively. Afterwards, titanium ter-butoxide was added drop by drop during two hours, maintaining a constant temperature of 70°C. After appropriate gelation, the samples were annealed at 200°C, 400°C, 600°C and 800°C subject to airflow during 4 hours.

Characterization

The X-Ray diffraction (XRD patterns were taken after the annealing process, in a Siemens D-5000 X-ray diffractometer with a Cu K radiation source (λ=0.15418 nm) operating at 40 kV. Diffraction intensities were obtained at angles 2θ between 10 and 70 degrees.

Electron Paramagnetic Resonance (EPR) spectra were obtained at room temperature, using a conventional reflection-type spectrometer with a cylindrical cavity (Model JES-RE3X, JEOL, Tokyo, Japan) (in TE a 011 mode) that was operating at a field modulation of 100 kHz. The "g" values were obtained by measuring the resonance field with a calibrated nuclear magnetic resonance (NMR) gaussmeter (Model ES-FC5, JEOL) and a frequency counter (Model HP-5350B, Hewlett–Packard, Palo Alto, CA). For the EPR measurements, the thermal treatments were performed in a controlled atmosphere furnace in which the sample was maintained at the appropriate temperature in the quartz tube, to avoid any influence from the external atmosphere. The pressure of the flowing gas was slightly higher than the atmospheric pressure during sample cooling to room temperature and the respective EPR measurement. The specific surface areas of the annealed materials were calculated from N_2 isotherms, obtained with an ASAP 2000 Micromeritics apparatus. The BET and BJH methods were used to calculate the specific areas and the mean pore diameter, respectively.

Infrared (FTIR) spectra were recorded in the wavenumber region 400-4000 cm^{-1}, on a Perkin Elmer Paragon 1000 spectrophotometer with a TGS detector. Wafers were obtained by mixing 10% of each material with 90% of KBr. Micro-Raman spectra were recorded at room temperature in a nearly backscattering geometry with a Jobin-Yvon Labram apparatus, equipped with a xy motorized stage and autofocus.

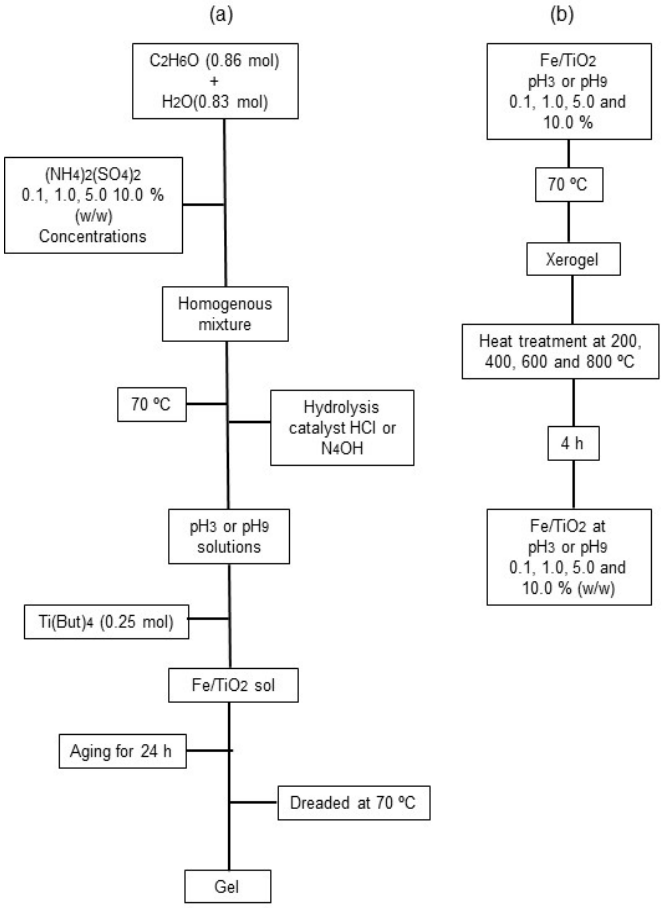

Figure 3: Diagram of sol-gel preparation method.

The excitation lines were the 632.8 nm line of a He-Ne laser and the 784.8 nm line of a laser diode. The laser power on the samples was kept low by using neutral density filters. Due to the possible heterogeneity of the samples, different measurements were performed on each one.

The samples treated at 200°C, brown in aspect, show a huge fluorescence in the visible and NIR ranges, so no useful Raman spectra were obtained for these samples.

The catalytic activity in the combustion of toluene was evaluated in a conventional flow reactor at atmospheric pressure using 100 mg of catalysts mixed with 200 mg of quartz as diluent to avoid thermal effects and a space velocity of 6000 h^{-1}. The activity was measured on the calcined samples (at different temperatures) from 90°C up to the temperature required for a total conversion using a heating rate of 10°C min^{-1}. Additional experiments were carried out over samples pre-reduced in situ under flowing H_2 (50 cm^3 g^{-1}) up to 500°C for 1 h. Then, after cooling down to 200°C, the reducing gas was switched to He (employed as carrier gas) and after 30 min of stabilization at this temperature, the carrier gas was switched to the reactant gaseous mixture containing toluene (1 vol%), O_2 (2 vol%) and He (balance). The effluents of the reactor were analyzed on-line with a gas chromatograph. A column containing molecular sieve (5A) was used. The chromatographic separation was carried out isothermally at 60°C with helium as carrier gas.

Results

X-ray diffraction

Figure 4 shows the diffractograms of Fe-TiO_2-pH_3-5.0% $FeCl_3$, and annealing at 200°C, 400°C, 600°C and 800°C. The fresh sample diffractogram presents only a thick line with a maximum at 2θ = 25° which indicates the presence of nanocrystalline anatase particles. Samples treated until 600 °C showed anatase peaks, which are rising by temperature increase. the sample at 800°C is more crystallized and presents an anatase, rutile and pseudobrookite mixture [12].

In Figure 5 is shown the crystallite sizes vs. temperature of the samples prepared with $FeCl_3$ and calcined at different temperatures. The crystalline size grows as the calcination temperature increases, over every sample. The crystallite size is larger in samples calcined at 800°C than in samples calcined at 200°C. For all catalysts, the crystallite size

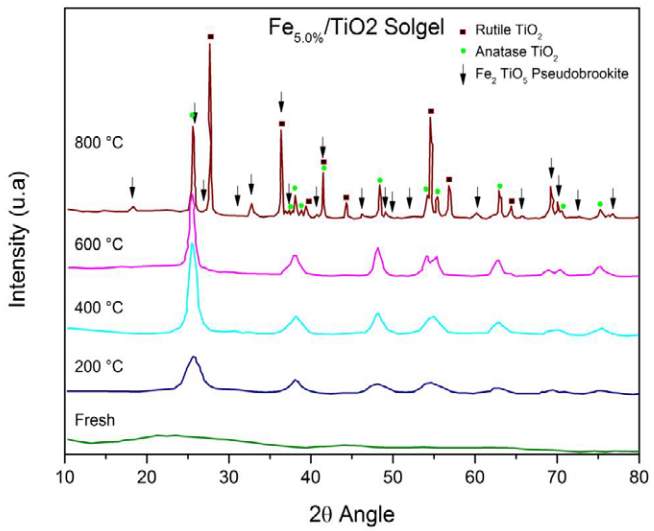

Figure 4: X-ray diffractograms of Fe-TiO_2-pH3-5.0% $FeCl_3$, annealing at different temperaturas.

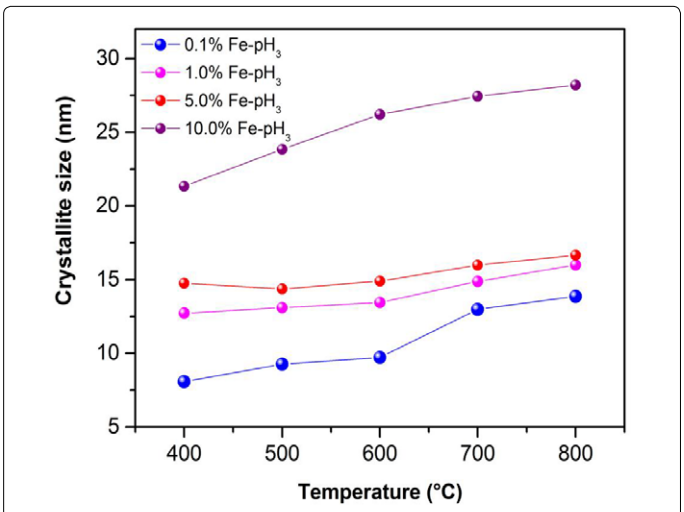

Figure 5: Graph of crystallite sizes vs. temperature of $FeCl_3$ prepared samples calcined at different temperatures.

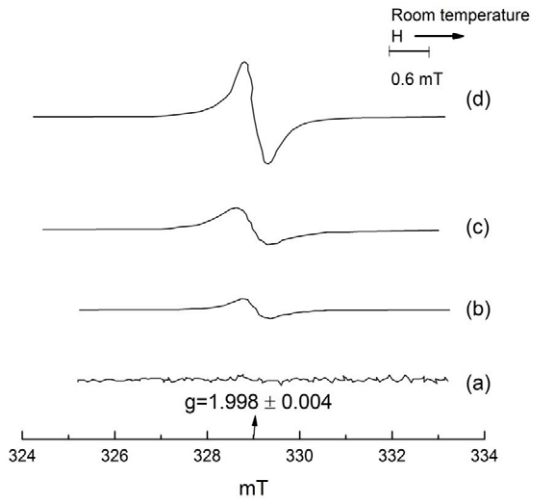

Figure 6: Room-temperature EPR spectra of the Ti_3^+ ions in so^l– gel derived TiO2 powder (Spectrum "(a)") corresponds to the fresh sample; all other samples were treated at 400°C for 15 min in either an oxygen flow spectrum "(b)", an argon flow (spectrum "(c)"), or a hydrogen flow (spectrum "(d)"). Theg-factor for spectra (b)–(d) was 1.99860.004. For all samples, the magnetic-field modulation was 0.08 mT.

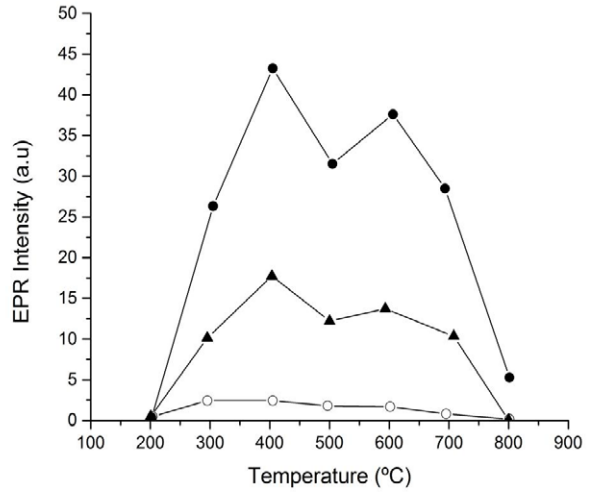

Figure 7: EPR signal intensity of the Ti_3^+ ions in sol$^-$ gel-derived TiO_2 powder, as a function of annealing temperature; the samples were subjected to three different gas atmospheres: (black spheres) hydrogen gas, (triangles) argon gas, and (empty circles) oxygen gas.

was between 8 and 30 nm, remaining nanocrystalline in the studied temperature range.

Electron Paramagnetic Resonance (EPR)

The inclusion of hydroxyl ions resulted in vacancies in the TiO_2 lattice and apparently provoked a further splitting of the energy levels of the ground-state Ti^{3+} ion, which produced EPR signals at higher temperatures than those reported for conventional TiO_2. However, Ti^{3+} EPR signals recently were observed in the functionalized phosphate nanoparticles at room temperature [13]. Even more striking was the phenomena shown in Figure 6 after TiO_2 was annealed in reducing, neutral, and oxidizing atmospheres. For comparison, curve "(a)" in Figure 6 shows the EPR spectrum of the fresh sample under oxygen atmosphere; no appreciable signal was observed (even at a high amplifier gain). Curves "(b)," "(c)," and "(d)" in Figure 6 show the EPR spectra of samples that have been treated at 400°C for 15 min in atmospheres of oxygen, argon, and hydrogen, respectively. One single first-derivative absorption line (line width of 0.6 mT) with g=1.998 ± 0.004 appeared in all three traces as the only signal over the scanned magnetic field (200 mT). The spectra of the annealed samples were measured with the same amplification and field modulation; however, the spectrum for the fresh sample was taken with a gain factor that was 200 times larger than that of the other samples. In all cases, the signal was similar, albeit of different intensity (compare curves (b)–(d) in Figure 6.

Naturally, the EPR signal was caused by the hydrogen that was contained in the sample. The amplitude of the signal for the sample treated in argon diminished substantially and even more so for that treated in the oxidizing atmosphere. Therefore, we may conclude that the presence of hydrogen enhanced the formation of Ti^{3+} ions and the presence of oxygen hindered but did not inhibit the production of Ti^{3+} ions. Under the current experimental results, this is direct evidence of the formation of Ti^{3+} ions. Naturally abundant titanium is composed of different isotopes; among these species, the even–even isotopes constitute the major contribution, although Ti(I=5⁄2) and Ti(I=7⁄2) respectively represent 7.75% and 5.51% of the total content. Indeed, the signals that are reported in Figure 6 correspond exclusively to even–even isotopes. The limited signal to noise ratio that is ascribed to the sol–gel preparation process contributed to the large spread in magnetic field of the expected broad hyperfine contribution of the titanium isotopes, which prevented the observation of hyperfine spectra.

Figure 7 shows the results of the thermal treatment to which the samples were subjected. The reported intensity represents the peak-to-peak height of the first derivative of the adsorption EPR curve, normalized to the weight of the sample. Intensity measurements were performed from room temperature up to 800°C, in increments of 200°C. The sample was held at the specific temperature for 15 min in the indicated gas flux before its EPR measurement. For all three gases, the threshold temperature at which Ti ions appeared was observed to be 200°C. From 200°C up to 400°C, the corresponding EPR signal increased monotonically until a maximum was attained. After this, the intensity of the Ti^{3+} signal decreased and, at 500°C, it began to increase again until a secondary maximum was attained. Further increases in temperature rapidly decreased the formation of Ti^{3+} ions, which was practically negligible at 800°C. The most significant conclusion of these results is the large stability of the Ti^{3+} signal at such high temperatures, especially under a hydrogen flux, but surprisingly even for the case of the samples treated in oxygen.

N_2 adsorption-desorption isotherms

Nitrogen adsorption-desorption isotherms were performed for all the materials, which according to IUPAC classification correspond to type IV isotherm characteristic of mesoporous xerogels (isotherms not shown). From the isotherms was calculated the surface area using the BET equation and the pore diameter with the BJH approximation [14] and the values are presented in Figure 8. It is clearly shown that the specific surface area drastically decrease when the annealing treatment is increased, independently of pH and the iron concentration used. In general, the surface areas are reduced from 200 m^2/g for samples treated at 200°C until 5 m^2/g for samples treated at 800°C. In contrast, the pore diameter increases when the annealing temperature is elevated. The temperature increment permits the gradual elimination of the solvent, of water and organic residues that are present in these

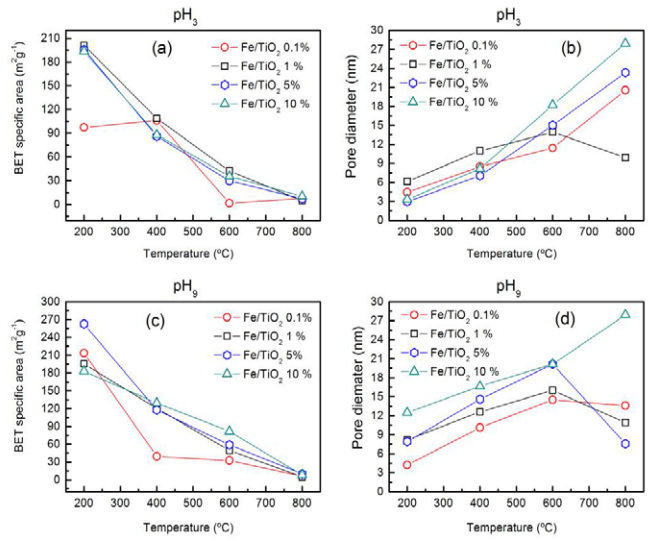

Figure 8: Graphics of the surface area BET and Pore diameter vs. temperature treatment of Fe-TiO_2 samples with different iron concentrations.

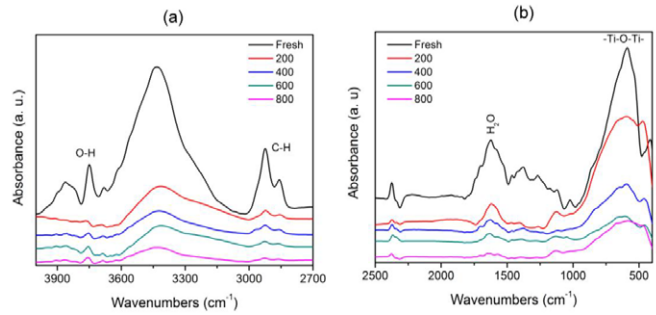

Figure 9: Sectioned infrared spectra of the Fe-TiO_2 materials prepared at pH3 with 1.0% of iron in function of the calcination temperature. (a) Stretching vibrations of OHs groups, (b) FTIR spectra at low energy.

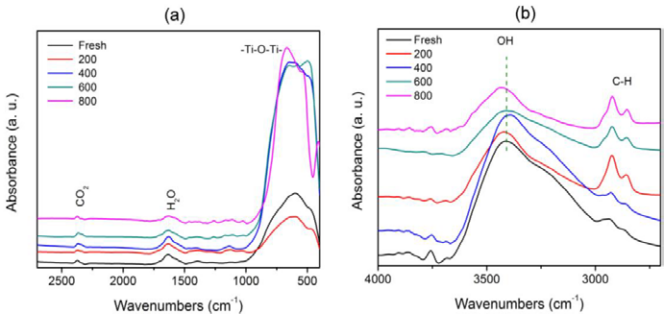

Figure 10: Sectioned FTIR spectra of Fe-TiO_2 with 1.0% of iron and prepared at pH9. (a) Stretching vibrations of OH, (b) FTIR at low energy.

materials and, consequently the deshydroxylation surface and sintering of Titania. These processes involved in the heat treatment of powders create intermolecular forces inside the cavities and the subsequent deformation and transformation of the crystal. In this case, there is a gradual transformation of phases from pseudo-amorphous passing to anatase to become a phase mixture (rutile, brookite and anatase) with their corresponding crystal enlarging. The sintering process usually generates dense polycrystalline solids with large sizes. Therefore, the samples treated at high temperatures (800°C) contain aggregates of large crystals, which generate large pores.

Infrared FTIR

Figure 9 shows the sectioned infrared spectra of the Fe-TiO_2 materials prepared at pH_3 with 1.0% of iron in function of the calcination temperature. In the high wavenumber region is observed a broad band at 3388 cm^{-1} and small absorptions at 3755 and 3855 cm^{-1} which correspond to stretching vibrations of OH (Figure 9a). The last two are related with Brönsted and Lewis acidity and these remain even at 800°C revealing the high stability of such OH's. When the annealing temperature is increased at 800°C the intensity of all the bands decreases due to deshydration and deshydroxylation processes of the material. The small bands located at 2921 and 2931 cm^{-1} are assigned to stretching vibrations of CH_2 and CH_3 of organic residual mater (solvent and alkoxide precursor), which are almost imperceptible at 600°C. This effect could be due to an increase of the interaction force between species due to the dehydration and dehydroxylation of the material. Figure 9b shows the FTIR spectra at low energy.

The band observed at 1639 cm^{-1} a band is observed assigned to the bending mode of OH groups from water. The two bands at 1462 and 1379 cm^{-1} are derived by the scissoring and wagging modes of C-H bonds from titanium alkoxide and solvent (ethanol), which disappear as the temperature is increased beyond 800°C. The signals at 1423 and 1241 cm^{-1} are asymmetric and symmetric stretching vibrations ($-COO^-$) of the carboxilate ion. The low wavenumber part of the spectrum characterizes the metal-oxigen bonds (≡Ti-O-Ti≡) showing a strong and broad absorption centered near 592 cm^{-1}. Nevertheless, it includes a band at 476 cm^{-1} assigned to the flexion of Ti-O bonds [15,16]. In titania-Fe nanobiocatalyts, the intensity of the stretching and wagging vibrations of the OH groups of water and solvents, of CH groups and Ti-O diminish and shifts towards higher wavenumbers. This effect could be related to an increase of the interaction force between species due to the deshydroxylation of the material.

The Figure 10 shows the sectioned FTIR spectra of Fe-TiO_2 with 1.0% of iron and prepared at pH_9. It seems to be similar to the sample prepared pH_3. Thus, we can see the signals corresponding to the different OHs types from water, alcohol, surface hydroxyls and Brönsted/Lewis hydroxyl acids (Figure 10). The signals that identified residual organic matter, from alkoxide and solvent, are observed between 2900 and 2750 cm^{-1}. However, it can be observed a shift of the absorption bands to higher wavenumbers and an intensity enhancement of these bands. This is due to a greater amount of surface OH groups in the material. When annealing temperature increases their intensity diminish due to the dehydroxylation process carried out in the material. However, the hydroxyls bands are appreciated even in the calcined sample at 800°C indicative of the high thermal stability of the OHs produce by the sol-gel method. In the lower region we clearly observe the peaks corresponding to water (1636 cm^{-1}), and ≡Ti-O-Ti≡ bonds (900-400 cm^{-1}), both previously explained.

Raman spectroscopy

Fe-TiO_2 1%, pH_3: The Raman spectra of the samples containing 1.0% of iron and prepared at pH_3 are shown in Figure 11a. The spectrum of the sample dried at 70°C (fresh) display broad bands centered in 152 cm^{-1} and is typical of the amorphous titania [17] but the main feature is typical of the anatase phase, very broaded and shifted with respect that of the bulk crystals [12-18]. This indicates the presence of very

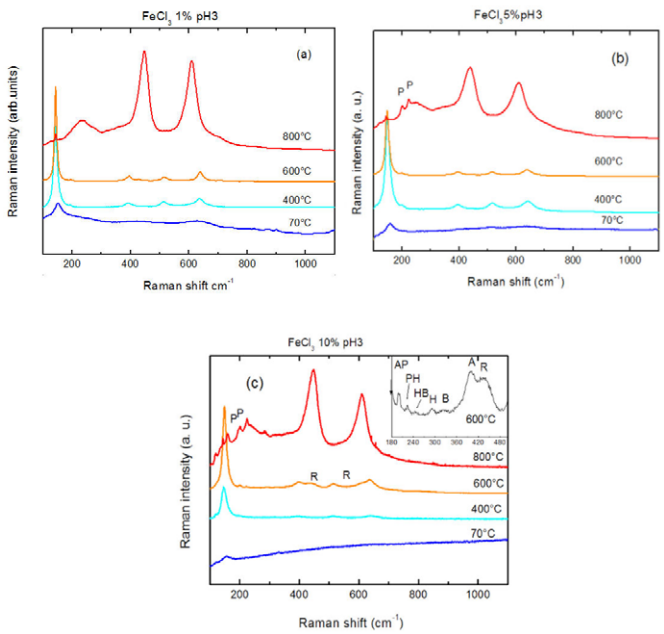

Figure 11: Raman spectra of samples prepared at pH3 with different concentration of iron and different thermal treatment.

		70°C	400°C	600°C
pH_3	1%	153 – 31 < 5 nm	145 – 13.5 10 nm	143.5 – 9 23 nm 144.5 – 11.5 14 nm
	5%	159 - 0. 26 < 5 nm	147 – 17 7 nm	149 – 15.5 8 nm
	10%	156 – 29 < 5nm	148 – 18 6 nm	144 – 11 15 nm 148 – 17 7 nm
pH_9	0.1%	-	-	144.5 – 10 18 nm
	1%	148.5 – 21 5 nm	146 – 14 9 nm	143.5 – 9.5 20 nm
	5%	150.5 -. 28 < 5 nm	150.5 – 18 6 nm 155 – 22.5 < 5 nm	145.5 – 13 10 nm
	10%	151 – 29 < 5nm	149 – 17 7 nm	145 – 13 10 nm

Table 1.Raman shift (cm^{-1}, ± 1 cm^{-1}) and FWHM (± 0.5 cm^{-1}) of the main anatase Raman band and estimated crystal size (nm, ± 25%) for the different samples. Different values are reported for the samples with high size dispersion.

small anatase nanocrystals or, at least, an anatase-like short range structure. Some sharp peaks, indicating the presence of organics, are visible at higher frequencies (200-1100 cm^{-1}) and disappear as the treatment temperature increases. The sample treated at 400°C show the Raman features of a nearly pure anatase phase; only in few points, a very weak band is hardly detectable at about 244 cm^{-1} indicating the presence of traces of brookite [19]. The anatase main Raman band is slightly broadened and shifted with respect the bulk values, due to the nanocrystalline form of the anatase powders [20,21]. The sample treated at 600°C shows also the anatase features, with a small shift towards lower frequencies and sharpening, indicating the growth of the nanocrystals, and without traces of brookite. The Raman spectrum of the sample treated at 800°C is typical of the pure rutile phase [22,23].

Figure 11b report the Raman spectra of the samples prepared with the 5.0% Fe. The sample dried at 70°C displays a spectrum similar to the dried sample with 1.0% Fe. The samples treated at 400°C and 600°C show also a trend similar to that displayed by the samples with 1.0% Fe, with nanocrystalline anatase growing in size as the annealing temperature is increasing, but, in the 5.0% Fe case, the anatase mean crystal size is lower, as displayed by the larger shift and width of the anatase main Raman band. In Table 1 the position and the full width at half-maximum (FWHM) of the anatase main Raman band for all the samples are summarized, together with an estimation of the anatase nanocrystal size, done by using a phonon confinement model [20]. For samples in which a large degree of disorder is expected (mainly the 70°C samples) or when a high dispersion in crystal size is present, the dimensions resulting from the model could be slightly under-estimated. The presence of a minor brookite phase is more evident in the 5.0% Fe samples, as visible in Figure 11b, and remains also at 600°C. As in the 1.0% Fe case, at 800°C anatase and brookite disappear and the rutile phase is obtained, but with some additional bands, that correspond to that of pseudobrookite Fe_2TiO_5 [24].

The sample with 10% Fe treated at 70°C displays a weak anatase-like band that emerges from a strong fluorescence background (Figure 11c). The spectrum of the sample treated at 400°C is also very noisy, and we may only notice the presence of the nanocrystalline anatase, without any information about the possible presence of minor phases. The sample treated at 600°C seems very heterogeneous, because the position and FWHM of the Raman bands of anatase (which is the main phase) display large variations taking the spectrum in different points of the sample (in different powder grains or in different points of the same grain), indicating a large size distribution of the anatase nanocrystals. Moreover, four minor phases are present in that sample: rutile, brookite, hematite Fe_2O_3 and the iron-titania mixed phase pseudobrookite. The sample treated at 800°C contains rutile as the main phase, together with hematite and pseudobrookite.

Fe-TiO_2 1%, pH_9: The sample with 1.0% Fe dried at 70°C already shows the Raman spectrum of a nanocrystalline anatase (Figure 12a). Increasing the treatment temperature up to 400°C and 600°C, the anatase remains the main phase but traces of brookite are present at both temperatures. The anatase grains grow as the thermal treatment proceeds, as evident by the decrease of frequency and FWHM of the main anatase Raman band. At 800°C the rutile is the only TiO_2 phase present, but with some weak additional bands, that nearly correspond to that of hematite.

The samples containing 5.0% Fe (Figure 12b) show a behavior similar to that of the 1.0% Fe samples, with the nanocrystalline anatase as the main phase from 70°C to 600°C, with the nanocrystals that grow with the annealing temperature and with the presence of a minor brookite phase at 400°C and 600°C. The nanocrystal size is however lower than in the case of the 1.0% Fe samples at the same temperature. The 800°C sample contains rutile as main phase, together with pseudobrookite. A very similar trend is obtained for the 10.0% Fe samples, apart for the higher content of pseudobrookite at 800°C of treatment respect to that of the 5.0% Fe sample (Figure 11c).

The main effect of the increase of the iron content on the obtained crystalline phases is, the formation of the iron oxide hematite and, mainly, of the mixed iron-titanium oxide pseudobrookite which is always present in the 5.0% and 10.0% Fe samples treated at 800°C. The only case in which pseudobrookite is obtained at a lower temperature is in the 10.0% Fe sample obtained at pH_3 annealed at 600°C. The introduction of iron seems to slow down the anatase crystal growth;

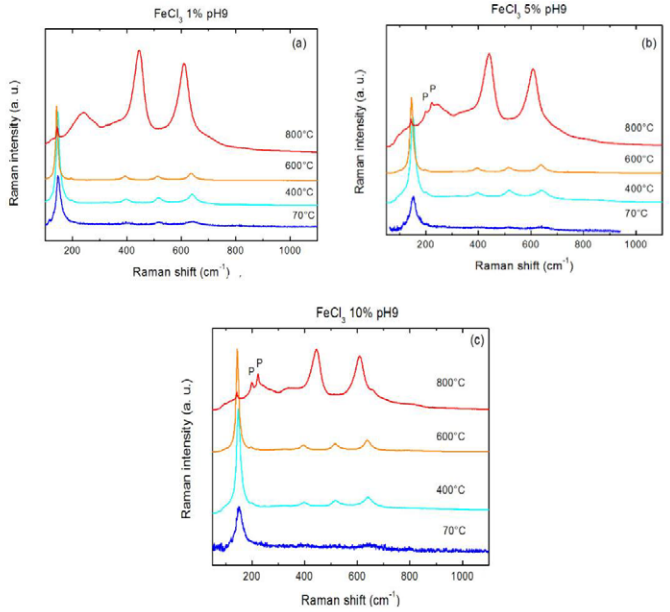

Figure 12: Raman spectra of samples prepared at pH9 with different concentration of iron and different thermal treatment.

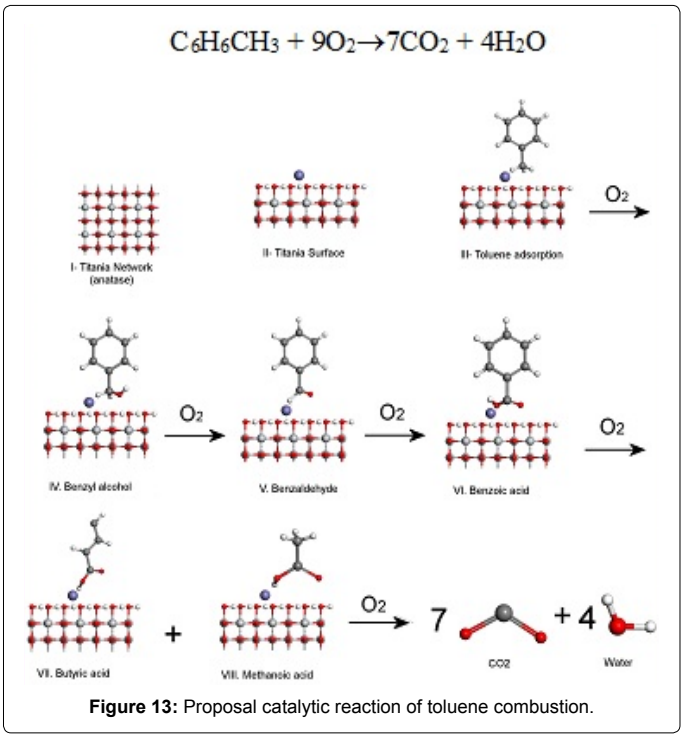

Figure 13: Proposal catalytic reaction of toluene combustion.

comparing samples obtained at the same pH and annealed at the same temperature, it is possible to observe that increasing the iron content the mean crystal size decrease. The effect is stronger passing from 0.1 to 1.0 and to 5.0% Fe, and weaker passing from 5.0 to 10.0% Fe. This can be due to the fact that iron compounds finely dispersed particles tends to be present at the anatase grain boundaries, making the grain growth by sintering more slow. At high Fe content, probably the iron and iron-titanium oxides segregate, and at higher temperature crystallize, and so the previous effect do not increase proportionally to the iron content (Figure 13).

Combustion

The DNA nitrogen bases contain mostly toluene, whose bonds have to be broken for our desired effects. These will break the C-C bonds in cancer cells, in the toluene combustion. This probe that our nanobiocatalysts also will broke the DNA bonds when we will do the "*in vivo*" tests.

The activities of toluene were measured as a function of the reaction temperature for a series of Fe-TiO_2 catalysts are given in Figure 14. The results demonstrated that complete reaction took place below 360°C. Apparently, the activity of conversion toluene increases according with the temperature and the global reaction carried out was (following scheme):

A complete conversion of toluene could be successfully achieved below 360°C over all nanobiocatalysts. The final products in the reaction were only CO_2 and H_2O. T_{50} corresponding to the temperature at 50% of toluene conversions. These values are used to compare the catalytic activities of the nanobiocatalysts and are summarized in Table 2. The Fe-TiO_2 catalyst prepared at pH_9 with a 1.0% exhibited the optimum catalytic activity with a T_{50} of 250°C. The ranking in terms of catalytic activity over all catalysts decreases as follows: Fe-TiO_2 (1.0% pH_9)>Fe-TiO_2 (5.0% pH_3)=Fe-TiO_2 (5.0% pH_9)>Fe-TiO_2 (1.0% pH_3). In the catalytic conversion, the catalysts prepared at pH_9 showed better catalytic activity than the catalysts prepared at pH_3. Independently of pH, the samples with 5.0% iron have the same catalytic activity. However, the sample with 1.0% of iron and prepared at pH_9 has better catalytic activity than that prepared at acid condition and with the same quantity of iron, which has the lower activity.

As is well known, since Watson and Crick [25], DNA molecules consist of two complementary chains of nucleotides. They are composed of sugar, phosphate groups and a base. The base may be adenine, cytosine, guanine or thymine.

These are joined by hydrogen bonds. A DNA molecule may contain

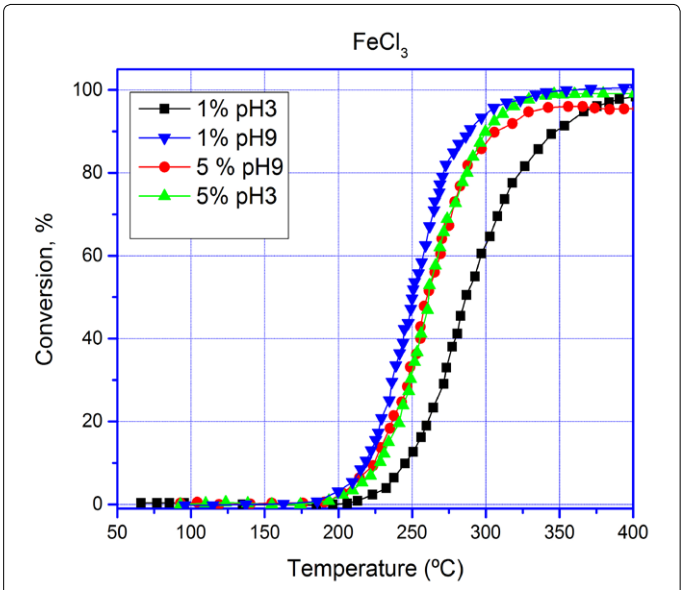

Figure 14: Conversion curves of the catalytic combustion of toluene on Fe-TiO_2 catalysts prepared at pH3 or pH9 with different iron content. The iron precursor was $FeCl_3$.

Catalyst	pH	% Fe	T_{50}, °C
$CuCl_3$			
Fe-TiO_2	3	1	286
Fe-TiO_2	3	5	261
Fe-TiO_2	9	1	250
Fe-TiO_2	9	5	261
$Cu(NH_4)_2(SO_4)_2$			
Fe-TiO_2	3	1	275
Fe-TiO_2	3	5	248
Fe-TiO_2	9	1	257
Fe-TiO_2	9	5	260

Table 2. T50 values corresponding to the temperature at 50% of toluene conversions.

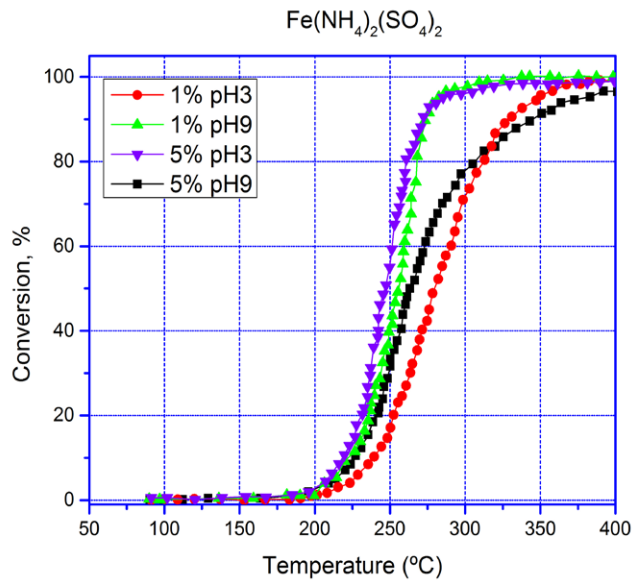

Figure 15: Conversion curves of the catalytic combustion of toluene on Fe-TiO_2 catalysts prepared at pH3 or pH9 with different iron content. The iron precursor was $Fe(NH_4)_2SO_4$.

three million base pairs long. These base pairs carry the code for the cell. How the pairs are arranged in the DNA make up the genetic code. The whole structure twists into a helix. The two ends link together to form a ring, and then the ring gets wadded up so it can fit inside the cell. In humans, is tightly wrapped into 23 pairs of chromosomes and also with distal sites called telomeres necessary for cell transcription.

The toluene rupture resembles DNA break up in C-C, H-H, N-N bonds arresting DNA transcription and protein assembly conditioning induction of cell apoptosis.

In Figure 15 we reported the catalytic conversion of toluene using $Fe(NH_4)_2(SO_4)_2$ based catalysts. Like the previous samples, the conversion of toluene increased with an increase in the reaction temperature and the complete combustion of toluene was achieved below 340°C with exception of the sample prepared at acid pH containing 1.0% of iron, which need a temperature of 400°C. The T_{50} values are summarized in Table 2. Among all, the Fe-TiO_2 catalyst prepared at pH_3 with a 5.0% exhibited the optimum catalytic activity with a T_{50} of 248°C. In this groups of nanobiocatalysts, the catalytic activity decreases as follows: Fe-TiO_2 (5.0% pH_3)>Fe-TiO_2 (1.0% pH_9)>Fe-TiO_2 (5.0% pH_9)>Fe-TiO_2 (1.0% pH_3). In the catalytic conversion, using the catalysts prepared at pH_9 showed better catalytic activity than the catalysts prepared at pH_3. On the other hand, the catalysts prepared at pH_9 presented similar catalytic conversion. Comparing the precursors used, catalysts $Fe(NH_4)_2SO_4$ were more efficient than the prepared with $FeCl_3$, because the $(NH_4)_2$ is decomposed and added to TiO_2 network.

Proposed catalytic reaction

The mechanism of catalytic reaction of toluene combustion carried out on Fe-TiO_2 catalysts is suggested in Figure 15. The titania network consists of the anatase phase which is the support of the iron metal (I). On the Fe-TiO_2 catalysts surface are iron atoms and terminal hydroxyl groups (II). In the catalytic process, the first step is the toluene adsorption on the catalyst surface (III) to be partially oxidized to benzyl alcohol (IV) by the oxygen used during the reaction. As there is an atmosphere with high oxygen content, the benzyl alcohol is further strongly oxidized to benzaldehyde (V), benzoic acid (VI), butyric acid and methyl acid; finally, mineralized to CO_2 and H_2O.

Conclusion

We present an experimental study of nanobiocatalyst materials, which we want to use for cancer treatment. Here was demonstrated the existence of Ti^{4+} and Ti^{3+} oxidation states, also Fe changes its oxidation state to Fe^{2+} and Fe^{3+}. We noticed that it never lost its octahedral structure and its coordination number of six. The particle sizes of anatase diminished when the iron content increase after 5% Fe due to formation of other phases like rutile, pseudobrookite, and hematite. These act as structuring of the titania network. These factors make that the samples at room temperature break the toluene becoming to CO_2 and H_2O. We expect very positive results when the nanocatalysts will be tested in Wistar rats (GBM models).

Acknowledgement

Conacyt, Uam-X, Uam-I, Innn, Ifunam Institutions, for the financial support.

References

1. Shi H, Magaye R, Castranova V, Zhao J (2013) Titanium dioxide nanoparticles: a review of current toxicological data. Part Fibre Toxicol 10: 15.
2. Wang JJ, Sanderson BJS, Wang H (2007) Cyto and genotoxicity of ultrafine TiO2 particles in cultured human lymphoblastoid cells. Mutat Res 628: 99-106.
3. Trouiller B, Reliene R, Westbrook A, Solaimani P, Schiest RH (2009) Titanium dioxide nanoparticles induce DNA damage and genetic instability in vivo in mice. Cancer Res 69: 8784-8789.
4. Pelaez M, Nolan NT, Pillai SC, Seery MK, Falaras P, et al. (2012) A review on the visible light active titanium dioxide photocatalysts for environmental applications. Appl Catal B Environ 125: 331-349.
5. Sikong L, Kongreong B, Kantachote D, Sutthisripok W (2010) Photocatalytic Activity and Antibacterial Behavior of Fe^{3+} -Doped TiO2/SnO2 Nanoparticles. Energy Res J 1: 120-125.
6. Ambrus Z, Balázs N, Alapi T, Wittmann G, Sipos P, et al. (2008) Synthesis, structure and photocatalytic properties of Fe(III)-doped TiO2 prepared from TiCl3. Appl Catal B Environ 81: 27-37.
7. Ewelina G, Hynd R, Adriana Z (2010) Photocatalitic Activity of TiO2 loaded with metal clusters. Physicochem Probl Miner Process 45: 29-38.
8. Ositadinma IM (2014) Ferritin and Serum Iron Levels among the ABO Blood Groups in Enugu, South Eastern Nigeria. J Blood Disord Transfus 5: 10-12.
9. Yu J, Yu H, Cheng B, Zhou M, Zhao X (2006) Enhanced photocatalytic activity of TiO2 powder (P25) by hydrothermal treatment. J Mol Catal A Chem 253: 112-118.
10. Hadjipanayis C, Bouras A, Chang S (2014) Applications of Multifunctional Nanoparticles in Malignant Brain Tumours. Eur Assoc NeuroOncology Mag 4: 9-15.

11. Ahmad S, Farrukh MA, Khan M, Khaleeq-ur- M, Tahir MA (2014) Synthesis of Iron Oxide-Tin Oxide Nanoparticles and Evaluation of their Activities against Different Bacterial Strains. Can Chem Trans 6458: 122-133.

12. So WW, Park S Bin, Kim KJ, Shin CH, et al. (2001) The crystalline phase stability of titania particles prepared at room temperature by the sol-gel method. J Mater Sci 36: 4299-4305.

13. Abraham MM, Bamberger CE (1991) Electron Paramagnetic Resonance Spectroscopic Determination of Ti3+ in Several Titanium Phosphate Compounds. Comun Am Ceram Soc 74: 2299-2300.

14. Sing KSW, Everett DH, Haul RAW, Moscou L, Pierotti RA, et al. (1985) Reporting Physisorption Data for Gas / solid Systems with Special Reference to the Determination of Surface Area and Porosity. Pure Appl Chem 57: 603-619.

15. Rao NN, Dube S, Natarajan P (1994) Photocatalytic reduction of nitrogen over (Fe, Ru or OS) / TiO, catalysts. Appl Catal B Environ 5: 33-42.

16. Nosheen S, Galasso FS, Suib SL (2009) Role of Ti-O bonds in phase transitions of TiO2. Langmuir 25: 7623-7630.

17. Su J, Zou X, Li GD, Jiang YM, Cao Y, et al. (2013) Room-temperature spontaneous crystallization of porous amorphous titania into a high-surface-area anatase photocatalyst. Chem Commun (Camb) 49: 8217-8219.

18. Djaoued Y, Badilescu S, Ashrit PV, Bersani D, Lottici PP, et al. (2002) Study of Anatase to Rutile Phase Transition in Nanocrystalline Titania Films. J Sol Gel Sci Technol 24: 255-264.

19. Iliev MN, Hadjiev VG, Litvinchuk A (2013) Raman and infrared spectra of brookite (TiO2): Experiment and theory. Vib Spectrosc 64: 148-152.

20. Bersani D, Lottici PP, Ding X-Z (1998) Phonon confinement effects in the Raman scattering by TiO[sub 2] nanocrystals. Appl Phys Lett 72: 73.

21. Bersani D, Antonioli G, Lottici PP, Lopez T (1998) Raman study of nanosized titania prepared by sol-gel route. J Non Cryst Solids 232-234: 175-181.

22. Swamy V, Muddle BC, Dai Q (2006) Size-dependent modifications of the Raman spectrum of rutile TiO[sub 2]. Appl Phys Lett 89: 163118.

23. Mazza T, Barborini E, Piseri P, Milani P, Cattaneo D, Li Bassi A, et al. (2007) Raman spectroscopy characterization of TiO2 rutile nanocrystals. Phys Rev B 75: 045416.

24. Bersani D, Lottici PP, Montenero A (1999) Micro-Raman Investigation of Iron Oxide Films and Powders Produced by Sol - Gel Syntheses. J Raman Spectrosc 30: 355-360.

25. Watson J, Crick FHC (1953) Molecular structure of nucleic acids: A structure for Deoxyribose Nucleic Acid. Nature 4356: 737-739.